Structure design and performance analysis of aerostatic thrust bearing with compound restrictors

Yuntang Li*, *Yueliang* Ye, *Ruirui* Li, *Pengfeng* Wang and *Fangfang* Zhang

College of Mechanical and Electrical Engineering, China Jiliang University, Hangzhou, China

Abstract. Aerostatic thrust bearing compensated by multi-orifices and porous material restrictor simultaneously is proposed to improve the static performance of the bearing. Load Carrying Capacity (LCC), stiffness and the flow field characteristics of the bearing are obtained by Computational Fluid Dynamic (CFD) simulation. The influences of supply pressure, orifice number, orifice diameter, orifice distribution, porous material thickness and permeability coefficient on the bearing performance are analysed. It is indicated that LCC and stiffness of the bearing with compound restrictors are much higher than those of the bearing with porous material restrictor or multi-orifice restrictor if gas film thickness is in rational range. The bearing with compound restrictors has better stability than that of the bearing with multi-orifice restrictor. Moreover, the optimum bearing parameters with compound restrictors are given to improving the performance of aerostatic thrust bearing.

Keywords: Aerostatic thrust bearing, Compound restrictors, Computational fluid dynamic, CFD, Load carrying capacity, LCC, Stiffness.

1 Introduction

Aerostatic thrust bearing is widely used in ultra-precision machining and measuring equipment because of its advantages of high speed, ultra-precision and slight friction. However, the development of machining and measuring technologies requires large **LCC**, high stiffness and better stability of aerostatic bearing. Many literatures engage to improve the static and dynamic performances of aerostatic bearing by performance analysis and structure optimization.

Zheng et al. [1] investigated the pneumatic hammer stability of aerostatic thrust bearing considering the delay effect and explained the reasons for pneumatic hammer phenomenon. Ishibashi et al. [2] compared experiments with the static and dynamic characteristics of downsized aerostatic bearing obtained by **CFD** simulations and those acquired by solving Reynolds equation. The results indicated that **LCC** and stiffness calculated by **CFD** were

* Corresponding author: yuntangli@cjlu.edu.cn

more consistent with experiments. Moreover, dynamic stiffness and dynamic damping coefficients obtained by **CFD** showed good match with experiments if average gas film thickness was less than 15μm. Li et al. [3] studied the stability of aerostatic thrust bearing with pocketed orifice-type restrictor by using large eddy simulation. The results indicated that the micro-vibration of the bearing could be restrained by decreasing orifice diameter and air chamber depth. Zhang et al. [4] pointed out that the nonlinear behaviours of aerostatic bearing could be restrained by adjusting the air supply pressure. Maamari et al. [5] presented a design reference ensuring the high stiffness and positive damping of aerostatic bearing based on the fluid-structure interaction model. Gao et al. [6] proposed an efficient fluid-structure interaction modelling method based on finite element method, which could reduce the average computation time from 9.36h to 86.2s. Zhang et al. [7] presented that the pressure depression in aerostatic bearing decreased with the decrease of supply pressure and average gas film thickness and the increase of orifice diameter and pressure ratio. Lai et al. [8] combined the flux-error feedback and optimization of grids parameter to calculate the performance of aerostatic bearing based on finite difference method. Moreover, the aerostatic bearing guideways made up of optical material were designed according to the optimum numbers and locations of orifices. Chen et al. [9]and Zha et al. [10] investigated the radial rotation error, dynamic stiffness coefficient, dynamic damping coefficient and the dynamic orbit of aerostatic bearing under the microscale effects.

Aerostatic thrust bearings with pocketed restrictor, inherent restrictor, slot restrictor and porous material restrictor have their distinguishing features. Moreover, the bearing with compound restrictors were taken into consideration in many researches. Cui et al. [11] investigated the dynamic performance of aerostatic thrust bearing with single orifice restrictor, multi-orifice restrictor and porous material restrictor, respectively. The results indicated that dynamic stiffness and dynamic damping coefficients of the bearing with porous material restrictor were significantly different from those of bearing with single orifice restrictor or multi-orifice restrictor. Ise et al. [12] proposed an externally pressurized gas journal bearing with eight slot restrictor for high-speed rotating machinery. The experiments showed that the rotor had no whirl vibration when rotation speed exceeded 22800rpm. Duan and Xu [13] verified that aerostatic thrust bearing made up of multi-microporous stainless steel plate had higher **LCC** by comparing experiments and **CFD** simulations. Wang et al. [14] studied influences of supply pressure, porous material thickness and Young's modulus on the deformation and static performance of aerostatic porous bearing by adopting fluid-structure interaction method. Wu and Tao [15] researched the static performance of aerostatic thrust bearing with porous material restrictor. They reported that stiffness could be increased by reducing porous permeability coefficient.

Hosokawa et al. [16] found that **LCC** of aerostatic thrust bearings with partial porous material restrictor decreased while stiffness improved compared to the bearing with traditional porous material restrictor. Silva et al. [17] used compound materials made of 0.4 wt.% of superplasticizer and 0.05 wt.% of carbon nanotubes as double-layered porous material restrictor in aerostatic thrust bearings and achieved acceptable bearing performance. Zheng et al. [18] experimentally verified that aerostatic thrust bearing compensated by a restrictor with multi-orifice series has higher maximal stiffness compared to the bearing with traditional orifice type restrictor. Gao et al. [19] investigated the effects of orifice length-diameter ratio on the performance of aerostatic thrust bearing by using **CFD**. Kodnyanko et al. [20] improved the dynamic performance of active aerostatic bearing by using elastic orifices. Rowe [21] presented a structure design of conical aerostatic journal bearing under high speeds. Gao et al. [22] analysed the effects of air chamber shapes on the performance of high speed aerostatic spindle by **CFD**. They concluded that **LCC** and stiffness varied with air chamber structure clearly.

In this paper, aerostatic thrust bearing with compound restrictors is proposed to fully

exploit the merits of orifice type and porous material restrictor. The flow characteristics inside the bearing is obtained. Moreover, the bearing stability is analysed according to the pressure fluctuation on the bearing surface. The influences of the supply pressure, orifice number, orifice diameter, orifice distribution, porous material thickness, porous material permeability coefficient and porous material diameter on bearing performance are discussed.

2 Aerostatic thrust bearing with compound restrictors

The structure of aerostatic thrust bearing with compound restrictors is shown in figure 1. Eight orifices evenly distributed in the porous materials. The restriction effect at the orifice outlet and porous material relates to LCC of the bearing.

The bearing performance is closely related to orifice diameter d, orifice distribution diameter d_0, air chamber diameter u, air chamber depth v, porous diameter D, porous thickness H, porous material permeability coefficient ψ, film thickness h and supply pressures (p_{s1} for porous material restrictor and p_{s2} for orifice restrictor). Compared to the bearing restricted by multi-orifice restrictor or porous material restrictor, it has more adjustable parameters for improving bearing performance.

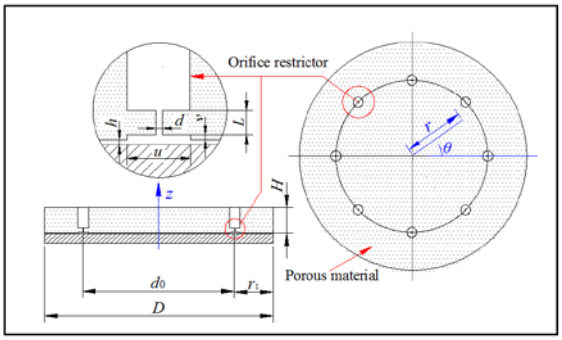

Fig. 1. Aerostatic thrust bearing with compound restrictors.

3 Numerical model

3.1 Numerical model for the bearing with multi-orifice restrictor

The pressurized gas effuses from orifice and gas pressure reduces to p_d from p_{s2}.It fills air chamber of orifice immediately and flows to atmosphere in the radial direction. Neglecting the flow in the circular and axial directions, the Naiver-Strokes equation in the cylindrical coordinate is

$$\begin{cases} \dfrac{\partial p}{\partial r} = \eta \dfrac{\partial v_r}{\partial z^2} \\ \dfrac{\partial p}{\partial \theta} = 0 \\ \dfrac{\partial p}{\partial z} = 0 \end{cases} \tag{1}$$

where v_r is the flow velocity in the radial direction, η is the dynamic viscosity coefficient of the lubricating gas. **LCC** of the bearing is

$$W = -\pi r_1^2 p_d \sqrt{\frac{G_1}{2}} \exp\left(\frac{2}{G_1}\right) \int_{\sqrt{\frac{2}{G_1}}}^{\frac{\sigma}{\beta}\sqrt{\frac{2}{G_1}}} \exp\left(-t^2\right) \mathrm{d}t \tag{2}$$

$$G_1 = \frac{1-(\sigma/\beta)^2}{\ln(2r_1/u)} \tag{3}$$

where $\beta=p_d/p_{s2}$, $\sigma=p_a/p_{s2}$, p_a is atmosphere pressure, r_1 is distance from the orifice center to the outer boundary of the bearing. Considering mass flow conservation, the pressure at orifice outlet can be written as

$$p_d^2 - p_a^2 = \frac{\varphi A n p_{s1}}{h^3} \psi' \sqrt{\frac{2}{p_a \rho_a}} \frac{12\eta p_a}{\pi} \ln\frac{R}{r_1} \tag{4}$$

$$\psi' = \begin{cases} \left[\dfrac{k}{k-1}\left(\beta^{2/k} - \beta^{(k+1)/k}\right)\right]^{1/2} & \beta > \beta_k \\ \left[\dfrac{k}{2}\left(\dfrac{2}{k+1}\right)^{(k+1)/(k-1)}\right]^{1/2} & \beta \le \beta_k \end{cases} \tag{5}$$

where A is orifice sectional area, n is orifice number, φ is flow coefficient, k is isentropic coefficient, β_k is critical pressure ratio, ρ_a is atmosphere density. p_d and W can be obtained by resolving equations (4) and (5).

The parameters of the multi-orifice restrictor are as follows: r_1=7.5mm, u=2mm, A=3.14×10^{-8}m^2, n=8, k=1.4, φ=0.8, β_k=0.528, ρ_a=1.205kg/m^3, p_a=0.1MPa and η=17.9×10^{-6}Pa·s.

3.2 Numerical model for the bearing with porous material restrictor

The flow velocity inside porous materials can be expressed according to Darcy's law

$$\begin{cases} u' = -\dfrac{\psi_r}{\eta}\dfrac{\partial p'}{\partial r} \\ v' = -\dfrac{\psi_\theta}{\eta}\dfrac{\partial p'}{\partial \theta} \\ w' = -\dfrac{\psi_z}{\eta}\dfrac{\partial p'}{\partial z} \end{cases} \tag{6}$$

where u', v' and w' are the flow velocity in the r, θ and z directions, respectively. p' is the gas pressure inside the porous material. ψ_r, ψ_θ and ψ_z are viscous permeability coefficients in the r, θ and z directions, respectively. Mass flow conservation equation of compressible gas is

$$\frac{1}{r}\frac{\partial\left(r\rho u'\right)}{\partial r}+\frac{1}{r}\frac{\partial\left(\rho v'\right)}{\partial\theta}+\frac{\partial\left(\rho w'\right)}{\partial z}=0 \tag{7}$$

By using transformation equation

$$p'\frac{\partial p'}{\partial r}=-\frac{\partial p'^2}{2\partial r} \tag{8}$$

The pressure distribution can be obtained inside the porous material

$$\frac{1}{r}\frac{\partial}{\partial r}\left(r\frac{\partial p'^2}{\partial r}\right)+\frac{1}{r^2}\frac{\partial^2 p'^2}{\partial\theta^2}+\frac{\partial p'^2}{\partial z}=0 \tag{9}$$

Considering the mass conservation equation, the pressure p in the film thickness is

$$\frac{1}{r}\frac{\partial}{\partial r}\left[rh^3\left(1+\xi\right)\frac{\partial p^2}{\partial r}\right]+\frac{1}{r^2}\frac{\partial}{\partial\theta}\left[h^3\left(1+\xi\right)\frac{\partial p^2}{\partial\theta}\right]=12\psi\left(\frac{\partial p'}{\partial z}\right)\Big|_{z=0} \tag{10}$$

where ξ is the slip flow factor and $\xi=3(2\psi+h\psi^{1/2}/k')/(h^2+h\psi^{1/2}/k')$. k' is dimensionless porous material slip coefficient. The boundary conditions are as follows: Atmospheric boundary condition: $p=p_a$ for $0\le\theta\le2\pi$, $r=D/2$ and $0\le z\le$h. Supply boundary condition: $p'=p_{s1}$ for $0\le\theta\le2\pi$ and $z=-H$. Continuity boundary condition: $p=p'$ for $0\le\theta\le2\pi$ and $z=0$. Seal boundary condition: $\partial p'/\partial r=0$ for $0\le\theta\le2\pi$, $r=D/2$ and $-H\le z\le0$.

LCC of the bearing can be calculated as

$$W=\int_0^{2\pi}\int_0^{2\pi}\left(p-p_a\right)r\mathrm{d}r\mathrm{d}\theta \tag{11}$$

4 Results and discussions

4.1 Flow field characteristics

FLUENT is used to analyze the flow characteristics inside the bearing. In order to improve mesh quality and calculation efficiency, one eighth of the bearing is considered because the bearing is periodic symmetry. Moreover, k-ε model in multi-orifice restrictor and laminar model in porous material restrictor are selected.

The boundary conditions and computational grid are shown in figure 2(a) and (b). There are two pressure inlets (orifice inlet and upper of porous materials), one pressure outlet, and two periodic surfaces. S is the section through the bearing center and orifice center. Line a-a is in the radial direction. Hexahedral element (Hex/Wedge) is used to mesh the model. There are much more grids in the air chamber of multi-orifice restrictor. The grid quality check results show that the mesh cell with EquiSize Skew between 0 and 0.4 is 99.74% and size change ratio less than 2 is 99.77%, which satisfy the requirements of calculation accuracy. The main calculation parameters of boundary conditions are listed in table 1 and bearing parameters are listed in table 2.

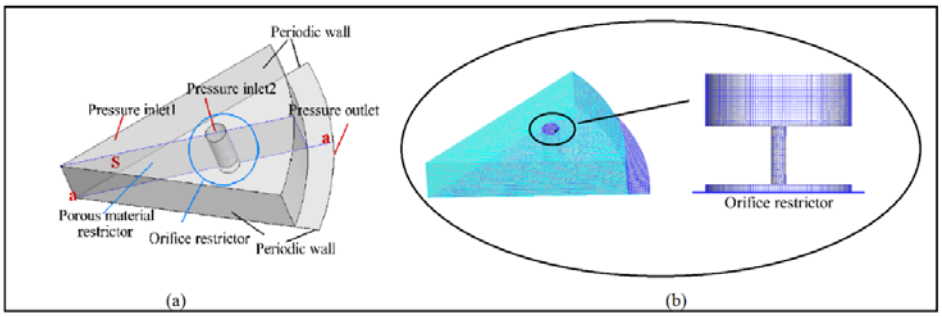

Fig. 2. Bearing modelling and meshing: (a) boundary conditions (b) computational grids.

Table 1. The main calculation parameters of boundary conditions.

Operation pressure (MPa)	0.101325	Inlet temperature(K)	293
Pressure inlet1 (p_{s1}) (MPa)	0.5	Outlet temperature(K)	293
Pressure inlet2 (p_{s2}) (MPa)	0.5	Ambient temperature(K)	293
Pressure outlet (MPa)	0		

Table 2. Bearing parameters with compound restrictors.

d (mm)	0.2	d_0 (mm)	30
L (mm)	0.8	n (mm)	8
u (mm)	2	D (mm)	45
v (mm)	0.1	H (mm)	5
ψ (m^2)	7.62×10^{-15}	h (μm)	20

The flow filed characteristics inside the bearing with compound restrictors are shown in figure 3. It can be seen from the figure 3(a) that the gas pressure at bearing center and near orifice outlet is much higher than that at other positions. figure 3(b) is the pressure distribution and streamlines of bearing with compound restrictors in section S. It is notable that the gas flow is reversed and the velocity reduces to 0m/s at a distance of 10.53mm (position A) from the bearing center along line a-a.

Influenced by the resistance of the countless feedholes inside the porous material, the gas velocity in the porous material is less than that in the multi-orifice restrictor. The gas effused from orifice radially flows to bearing outlet and bearing center simultaneously. When the flow field is steady state, the gas pressure at the outlet of the porous material restrictor will increase as shown in figure 3(a). The gas effused from porous material restrictor (yellow part) and that effused from the multi-orifice restrictor (blue part) meet at position A as shown in figure 3(b). Then the gas flows in the circumferential direction after changing flow direction as shown in figure 3(c) (streamlines). Therefore, the speed in the position A is 0m/s.

Vortices emerge in the air chamber of orifice restrictor at the distance of 0.1 mm from the orifice center. Usually, vortices cause pressure fluctuation on the bearing surface and induce the bearing to be micro-vibration, which seriously affects the stability of the bearing. In order to analyze the stability of the bearing, large eddy simulation is used to analyze the pressure fluctuation on bearing surface. It can be observed form figure 4 that the surface pressure fluctuation amplitude of the bearing is very small and the maximum amplitude is 0.803Pa.

The static performance of the bearing with compound restrictors and those of the bearing with traditional restrictor is also considered. The gas pressure distribution and streamlines inside the bearing with porous material restrictor and multi-orifice restrictor are shown in figure 5(a) and (b). It indicates that the flow field in gas film of porous material is

stable. However, vortices generate in the air chamber near orifice outlet. figure 5(c) and (d) shows the pressure fluctuation on the surface of bearing with porous material restrictor and that of the bearing with multi-orifice restrictor. The maximum amplitudes of pressure fluctuation are 1.3642×10^{9}Pa and 1026.81Pa, respectively. The bearing with porous material restrictor is the most stable. Although the stability of the bearing with compound restrictors is slightly lower than that of the bearing with porous material restrictor, it is more stable than the bearing with multi-orifice restrictor.

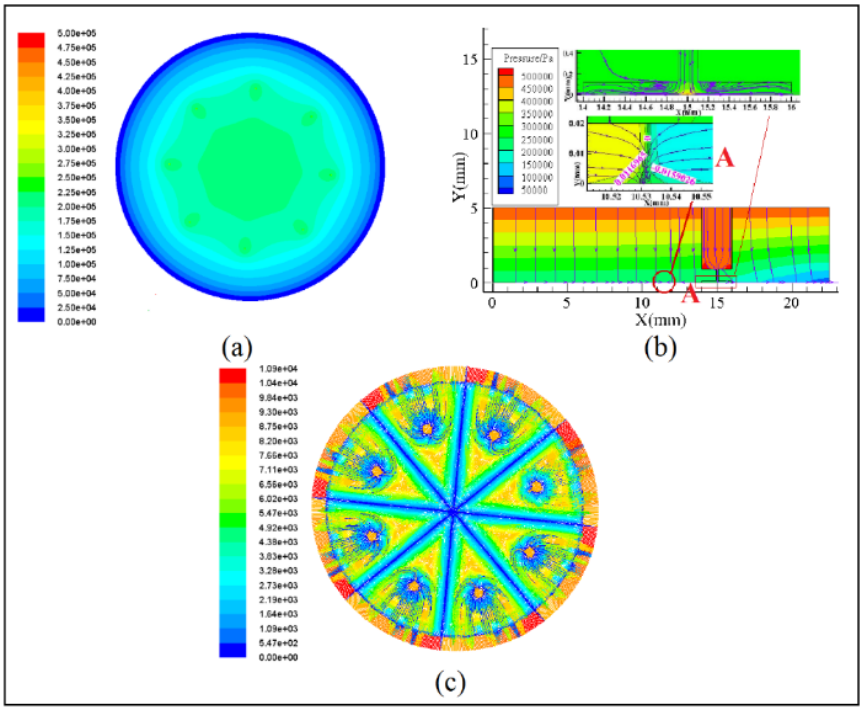

Fig. 3. Flow field characteristics of compound bearing: (a) gas film pressure distribution (b) flow field characteristic along the plan S (c) streamlines.

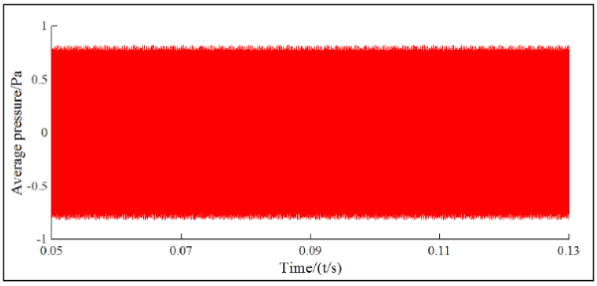

Fig. 4. Pressure fluctuation on the bearing surface.

4.2 Verification and comparison

The literatures [15] reports numeral experimental results of the bearing with porous material restrictor and orifice restrictor. The results of **CFD** software are compared with those of literatures [15] under the same boundary conditions and bearing parameters (listed

in table 3). The supply pressure is 0.6MPa, ambient pressure is 0.1MPa and ambient temperature is 293K.

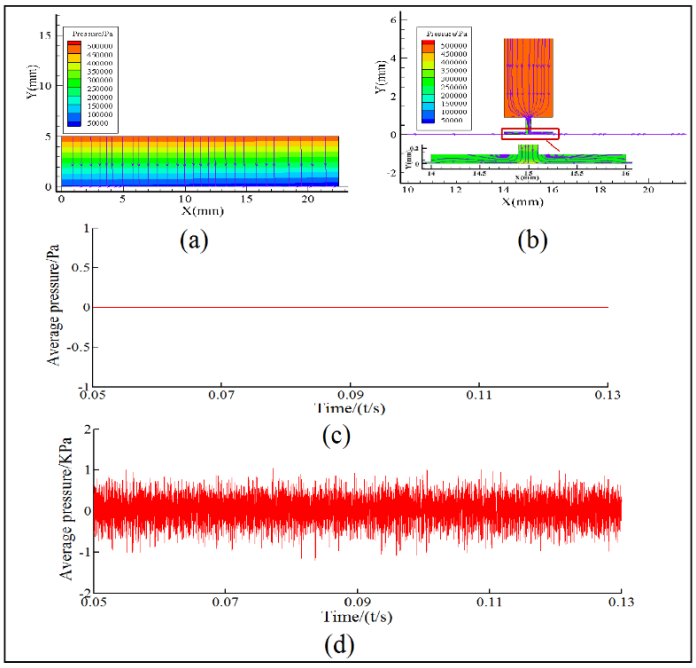

Fig. 5. Flow field characteristics of traditional bearings: (a) and (b) pressure distribution and streamlines contours (c) and (d) average pressure fluctuation on bearing surface.

Table 3. Bearing parameters of literatures [15].

Multi-orifice restrictor		porous material restrictor
d=0.2mm	L=2mm	D=45mm
u=3mm	v=0.02m m	H=10mm
d_0=30mm	n=8	ψ=7.877×10^{-15}m^2

Figure 6(a) and (b) are the results of **LCC** and stiffness of the bearing with porous material restrictor reported in the literatures [15] and calculated by **CFD** method. figure 6(c) and (d) are the results of **LCC** and stiffness of the bearing with multi-orifice restrictor reported in literatures [15] and calculated by **CFD** method. It can be seen that **CFD** results are very closely to those of the experiments reported in the literatures [15].

LCC and stiffness of the bearing with multi-orifice restrictor, porous material restrictor and compound restrictors are shown in figure 7(a) and (b), respectively. The bearing parameters are listed in table 2, the supply pressure is 0.5MPa, ambient pressure is 0.1MPa and ambient temperature is 293K. The bearing with compound restrictors has the highest **LCC** if the film thickness is less than 11μm. Stiffness is lower than that of the bearing with porous material restrictor, it is much higher than that of the bearing with multi-orifice restrictor. When film thickness is in the range of 11μm to 13μm, the bearing with porous material restrictor has higher stiffness and lower **LCC**, and the bearing restricted by multi-orifice restrictor has higher **LCC** and lower stiffness. However, **LCC** and stiffness of the bearing with compound restrictors are higher than that of the bearing with porous material restrictor or with multi-orifice restrictor. Therefore, the bearing with compound restrictors has better performance.

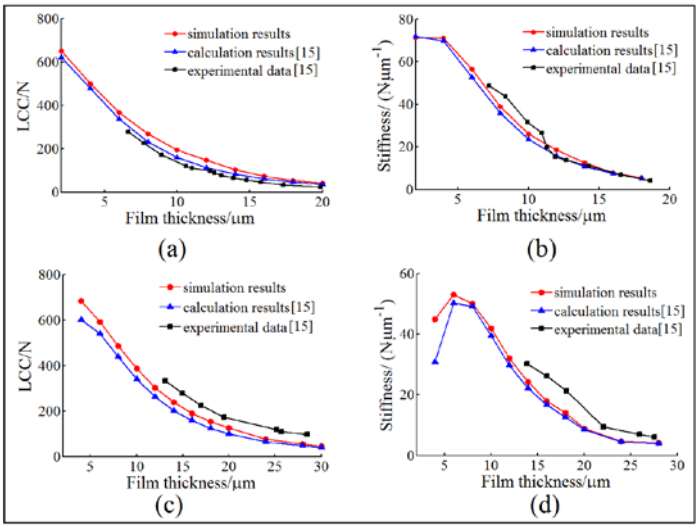

Fig. 6. Verification of the CFD results: (a) and (b) LCC and stiffness of bearing with porous material restrictor (c) and (d) LCC and stiffness of bearing with multi-orifice restrictor.

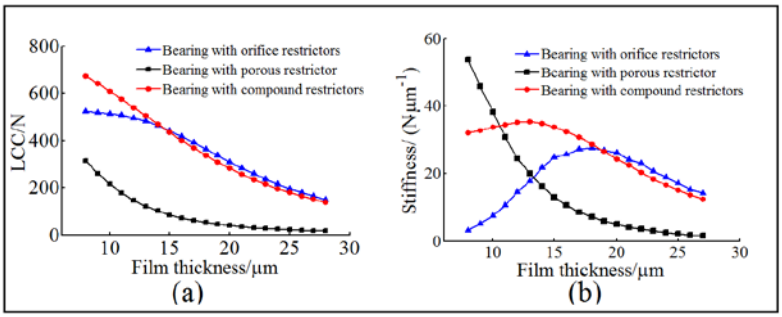

Fig. 7. Comparison of three type restrictor: (a) LCC, and (b) Stiffness.

4.3 Influence design parameters on bearing performance

The relationship between bearing parameters (listed in table 4) and its performance are analyzed by using the control variable method. The ambient pressure is 0.1MPa, ambient temperature is 293K, film thickness is in the range of 8μm to 28μm. It can be observed from figures 6 to 12 that the performance of the bearing with compound restrictors is influenced by porous material and orifice parameters simultaneously.

Table 4. Bearing parameters.

Bearing parameters	Initial value	Variation range
p_{s1}, p_{s2}(MPa)	0.5	0.4-0.6
n	8	4-8
d(mm)	0.2	0.2-0.4
d_0(mm)	30	15-30
H(mm)	5	3-8
ψ(m^2)	7.62×10^{-15}	7.62×10^{-15}-3.65×10^{-13}
D(mm)	45	37-45

Given the supply pressure of porous material restrictor is p_{s1} and that of multi-orifice restrictor is p_{s2}. **LCC** and stiffness of the bearing are shown in figure 8(a) and (b) when supply pressure p_{s1} is equal to p_{s2} and varies from 0.4MPa to 0.6MPa. **LCC** and stiffness increase significantly with the growth of supply pressure at the same film thickness. Moreover, **LCC** decreases with the growth of film thickness if supply pressure is changeless. However, stiffness increases firstly with the increase of film thickness, and then decreases after reaching the maximum value.

LCC and stiffness are shown in figure 8(c) and (d) when p_{s1} is not equal to p_{s2}. Compared to the condition of same supply pressure (0.4MPa), **LCC** of the bearing with multi-orifice restrictor in supply pressure 0.5MPa and porous material restrictor in supply pressure 0.4Mpa is higher than that of the bearing with multi-orifice restrictor in the supply pressure of 0.4MPa and porous material restrictor in supply pressure of 0.5Mpa. Moreover, the bearing stiffness firstly increases with the increase of film thickness, and then decreases when the film thickness is larger than 10μm.

Figure 9(a) and (b) indicate the effects of orifice number on bearing performance. With the growth of orifice number from 4 to 8, **LCC** increases obviously from 528.7N to 815.6N at the same film thickness of 8μm. The changing trend of bearing stiffness with orifice number alters when film thickness is 15μm. It decreases with the growth of orifice number if film thickness is less than 15μm while it increases if film thickness is larger than 15μm. Moreover, the film thickness corresponding to the maximum stiffness increases with the growth of orifice number.

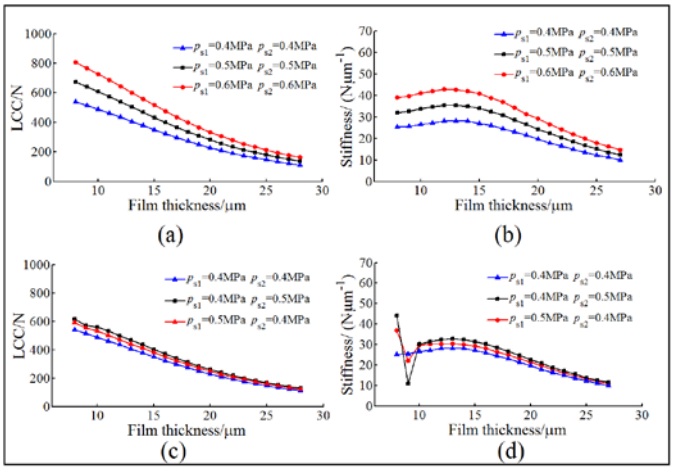

Fig. 8. Influence of Ps on bearing performance: (a) and (b) the same supply pressures (c) and (d) the independent supply pressures.

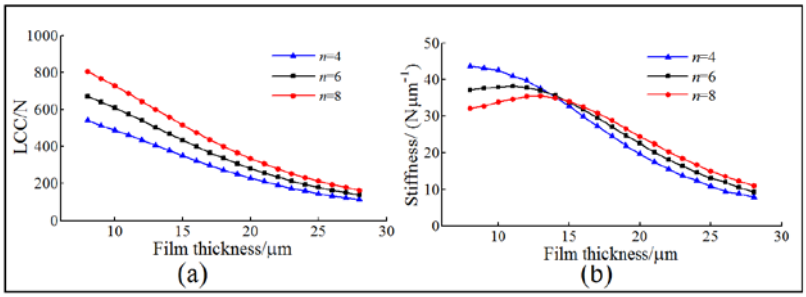

Fig. 9. Influence of n on bearing performance: (a) LCC, and (b) Stiffness.

The effects of orifice diameter on bearing performance are shown in figure 10(a) and (b). **LCC** increases with the growth of orifice diameter if film thickness is constant. The larger the film thickness is, the more clearly the influences of orifice diameter on **LCC** are. Stiffness increases significantly with the decreases of the orifice diameter if the film thickness is less than 20μm.

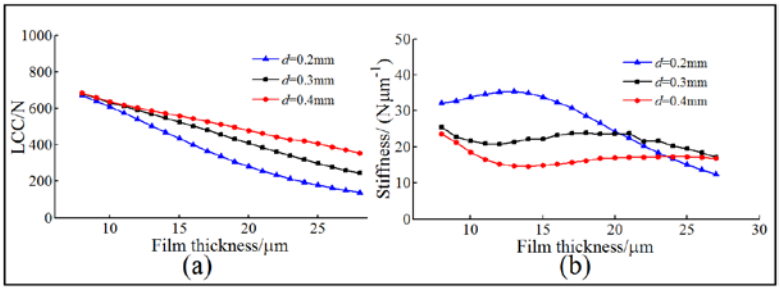

Fig. 10. Influence of d on bearing performance: (a) LCC, and (b) Stiffness.

Figure 11(a) and (b) show the influences of orifice distribution diameter on bearing performance. With the growth of orifice distribution diameter, **LCC** increases if film thickness is less than 17μm. Orifice distribution diameter has little effect on **LCC** if film thickness is in the range of 18μm to 28μm. Moreover, stiffness increases with the increase of orifice distribution diameter if film thickness is larger than 10μm and the influences of orifice distribution diameter on bearing stiffness can be ignored when the film thickness exceeds a certain value.

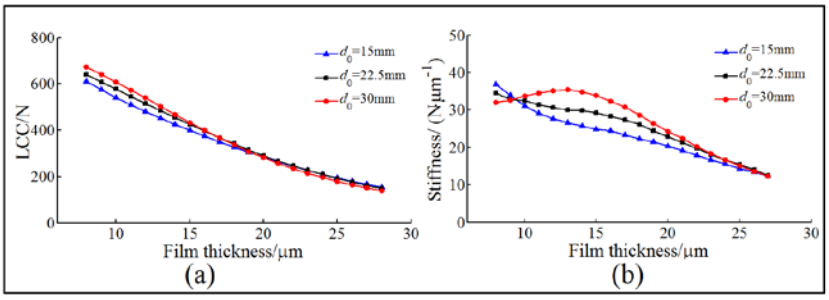

Fig. 11. Influence of d_0 on bearing performance: (a) **LCC** (b) Stiffness.

Figure 12(a) and (b) show the effects of porous material thickness on bearing performance. It can be seen that **LCC** monotonously decreases with the growth of porous material thickness if film thickness is constant. Stiffness increases with the growth of porous material thickness when film thickness is from 8μm to 16μm while it decreases if the film thickness is larger than 17μm.

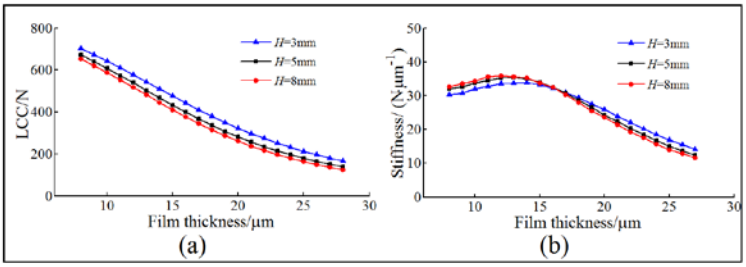

Fig. 12. Influence of H on bearing performance: (a) LCC (b) Stiffness.

The influences of porous material permeability coefficient on the bearing performance are shown in figure 13(a)and (b). **LCC** increases significantly from 672.3N to 858.2N and bearing stiffness decreases obviously from 32.1N to 6.9N with the growth of porous material permeability coefficient from $7.62\times10^{-15}m^2$ to $3.65\times10^{-13}m^2$ at the film thickness of 8μm. In addition, the smaller the porous material permeability coefficient is, the more obvious the change of bearing performance is.

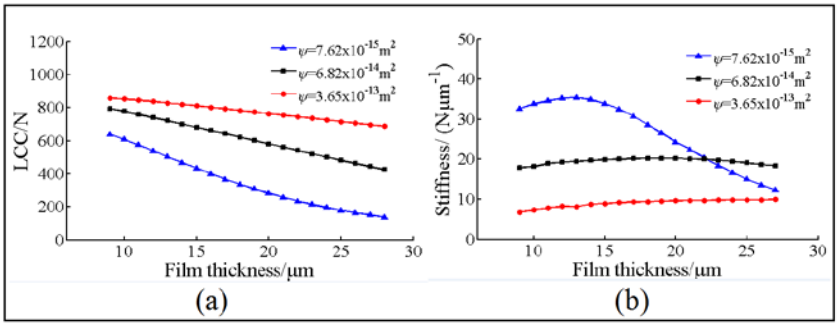

Fig. 13. Influence of ψ on bearing performance: (a) **LCC** (b) Stiffness.

Figure 14(a) and (b) indicate the effects of porous material diameter on bearing performance. It can be concluded that increasing porous material diameter can effectively improve the performance of the bearing. Both **LCC** and bearing stiffness reach the maximum value when porous material diameter is 53mm.

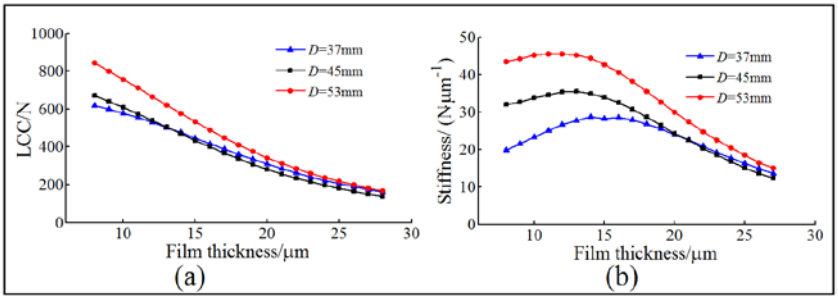

Fig. 14. Influence of D on bearing performance: (a) LCC (b) Stiffness.

5 Conclusion

A new type of high **LCC** aerostatic thrust bearing with compound restrictors is proposed. Flow field characteristics and bearing stability are analyzed by using **CFD** simulation. The validity of **CFD** results is carried out by existing experiments. Moreover, the effects of bearing parameters on its performance is discussed. Compared to the bearing restricted by multiple orifices or porous material restrictor, the flow field in the bearing with compound restrictors is complex. Although vortices emerge in the air chamber of orifice restrictor, the pressure fluctuation amplitude of the bearing with compound restrictors is very small. There the bearing is more stable than the bearing with multiple orifices or porous material restrictor.

Under the same operating conditions, **LCC** and stiffness of bearing with compound restrictors are improved clearly if film thickness is in a certain range. High supply pressure and large porous material diameter can improve the performance of the bearing with compound restrictors effectively. **LCC** increases with the increase of orifice number,

orifice diameter, porous material permeability coefficient and the decrease of porous material thickness. In small film thickness, stiffness increases with the decrease of orifice number, orifice diameter, orifice distribution diameter, porous material permeability coefficient and the increase of porous material thickness.

This study was sponsored by the National Nature & Science Foundation of China under grants 51675498 and 51275499, the Fundamental Research Funds for the Provincial Universities of Zhejiang under grant 2020YW29.

References

1. Zheng Y, Yang G, Cui H, et al. Pneumatic stability analysis of single-pad aerostatic thrust bearing with pocketed orifice[J]. *Proc IMechE, Part J: J Engineering Tribology*, 2020, 234(12): 1857-1866.
2. Ishibashi K, Kondo A, Kawada S, et al. Static and dynamic characteristics of a downsized aerostatic circular thrust bearing with a single feed hole[J]. *Precis Eng*, 2019, 60: 448-457.
3. Li Y, Zhao J, Zhu H. Numerical analysis and experimental study on the micro vibration of an aerostatic thrust bearing with a pocketed orifice-type restrictor[J]. *Proc IMechE, Part J: J Engineering Tribology*, 2014; 229: 609-623.
4. Zhang J, Han D, Song M, et al. Theoretical and experimental investigation on the effect of supply pressure on the nonlinear behaviors of the aerostatic bearing-rotor system[J]. *Mech Syst Signal Process*, 2021, 158
5. Maamari N, Krebs A, Weikert S, et al. Stability and dynamics of an orifice based aerostatic bearing with a compliant back plate[J]. *Tribol Int*, 2019, 138: 279-296.
6. Gao Q, Qi L, Gao S, et al. A FEM based modeling method for analyzing the static performance of aerostatic thrust bearings considering the fluid-structure interaction[J]. *Tribol Int*, 2021, 156.
7. Zhang J, Zou D, Ta N, et al. Numerical research of pressure depression in aerostatic thrust bearing with inherent orifice[J]. *Tribol Int*, 2018, 123: 385-396.
8. Lai T, Peng X, Liu J, et al. Design optimization of high-precision aerostatic equipment based on orifice restriction[J]. *Proc Inst Mech Eng C: J Mechanical Engineering Science*, 2019, 233(10): 3459-3474.
9. Chen D, Han J, Dong L, et al. An evaluation system of the eccentric orbit of shaft with aerostatic bearing in the microscale[J]. *Proc IMechE, Part J: J Engineering Tribology*, 2018, 232(2): 155-165.
10. Zha C, Li T, Zhao Y, et al. Influence of microscale effect on the radial rotation error of aerostatic spindle[J]. *Proc IMechE, Part J: J Engineering Tribology*, 2020, 234(7): 1131-1142.
11. Cui H, Wang Y, Yue X. Numerical analysis of the dynamic performance of aerostatic thrust bearings with different restrictor[J]. *Proc IMechE, Part J: J Engineering Tribology*, 2019; 233(3): 406-423.
12. Ise T, Nakatsuka M, Nagao K, et al. Externally pressurized gas journal bearing with slot restrictor arranged in the axial direction[J]. *Precis Eng*, 2017; 50:286-292.
13. Duan L and Xu M. Study on static performance of gas-lubricated thrust bearing based on multi-microporous stainless steel plate[J]. *J Braz Soc Mech Sci*, 2021, 43(5)
14. Wang W, Chen X, Zhang M, et al. Effect of the deformation of porous materials on the performance of aerostatic bearings by fluid-solid interaction method[J]. *Tribol Int*,

2020, 150.

15. Wu D, Tao J. Research on key technologies of porous aerostatic thrust bearings. *China Academy of Engineering Physics*, 2010(in Chinese).
16. Hosokawa T, Somaya K, Miyatake M, et al. Static characteristics of aerostatic thrust bearings with multiple porous materials inlet ports[J]. *J Tribol*, 2015; 137: 3698-3703.
17. Silva L, Panzera T, Vieira L. Carbon nanotubes and superplasticizer reinforcing cementitious composite for aerostatic porous bearing[J]. *Proc IMechE, Part J: J Engineering Tribology*, 2017; 11: 1397-1407.
18. Zheng Y, Yang G, Cui H, et al. Improving the stiffness of the aerostatic thrust bearing by using a restrictor with multi-orifice series[J]. *Proc IMechE, Part J: J Engineering Tribology*, 2020, 234(12): 1881-1891.
19. Gao S, Shang Y, Gao Q, et al. CFD-Based Investigation on Effects of Orifice Length-Diameter Ratio for the Design of Hydrostatic Thrust Bearings[J]. *Appl Sci*, 2021, 11(3), 959-977.
20. Kodnyanko V, Shatokhin S, Kurzakov A, et al. Theoretical analysis of compliance and dynamics quality of a lightly loaded aerostatic journal bearing with elastic orifices[J]. *Precis Eng*, 2021, 68: 72-81.
21. Rowe W B. Conical hydrostatic journal bearings for high speeds[J]. *Proc IMechE, Part J: J Engineering Tribology*, 2021, 235(4): 808-819.
22. Gao S, Cheng K, Chen S, et al. CFD based investigation on influence of orifice chamber shapes for the design of aerostatic thrust bearings at ultra-high speed spindles[J]. *Tribol Int*, 2015; 92: 211-221.